Title

A Novel Radioligand Reveals Tissue Specific Pharmacological Modulation of Glucocorticoid Receptor Expression with Positron Emission Tomography

Journal

ACS Chemical Biology, 15(6)

ISSN

1554-8929

Authors

Huang, Yangjie
Zhao, Ning
Wang, Yung-hua
et al.

Publication Date

2020-06-19

DOI

10.1021/acschembio.9b01043

Peer reviewed

ACS chemical biology

pubs.acs.org/acschemicalbiology

Articles

A Novel Radioligand Reveals Tissue Specific Pharmacological Modulation of Glucocorticoid Receptor Expression with Positron Emission Tomography

Yangjie Huang, Ning Zhao, Yung-hua Wang, Charles Truillet, Junnian Wei, Joseph E. Blecha, Henry F. VanBrocklin, Youngho Seo, Mohd Sayeed, Brian J. Feldman, Rahul Aggarwal, Spencer C. Behr, Hao Shao, David M. Wilson, Javier E. Villanueva-Meyer, Jason E. Gestwicki, and Michael J. Evans*

Cite This: *ACS Chem. Biol.* 2020, 15, 1381−1391

Read Online

ACCESS | Metrics & More | Article Recommendations | Supporting Information

ABSTRACT: The complexity of glucocorticoid receptor (GR) signaling cannot be measured with direct tissue analysis in living subjects, which has stifled our understanding of GR's role in human physiology or disease and impeded the development of selective GR modulators. Herein, we report ^{18}F-5-(4-fluorobenzyl)-10-methoxy-2,2,4-trimethyl-2,5-dihydro-1H-chromeno[3,4-*f*]-quinoline (^{18}F-YJH08), a radioligand that enables noninvasive measurements of tissue autonomous GR expression levels *in vivo* with positron emission tomography (PET). YJH08 potently binds GR (K_i ∼ 0.4 nM) with ∼100-fold selectivity compared to nuclear hormone receptors in the same subfamily. ^{18}F-YJH08 was prepared *via* $Cu(OTf)_2(py)_4$-mediated radiofluorination of an arylboronic acid pinacol ester with ∼12% decay corrected radiochemical yield from the starting ^{18}F-fluoride ion. We applied treatment with the tissue-wide GR agonist dexamethasone and adrenalectomy and generated an adipocyte specific GR knockout mouse to show that ^{18}F-YJH08 specifically binds GR in normal mouse tissues, including those for which aberrant GR expression is thought to drive severe diseases (e.g., brain, adipose tissue, kidneys). Remarkably, ^{18}F-YJH08 PET also revealed that JG231, a potent and bioavailable HSP70 inhibitor, selectively degrades GR only in the adipose tissue of mice, a finding that foreshadows how GR targeted PET might be integrated into drug discovery to screen for selective GR modulation at the tissue level, beyond the historical screening that was performed at the transcriptional level. In summary, ^{18}F-YJH08 enables a quantitative assessment of GR expression levels in real time among multiple tissues simultaneously, and this technology is a first step toward unraveling the daunting complexity of GR signaling and rationally engineering tissue specific therapeutic modulators *in vivo*.

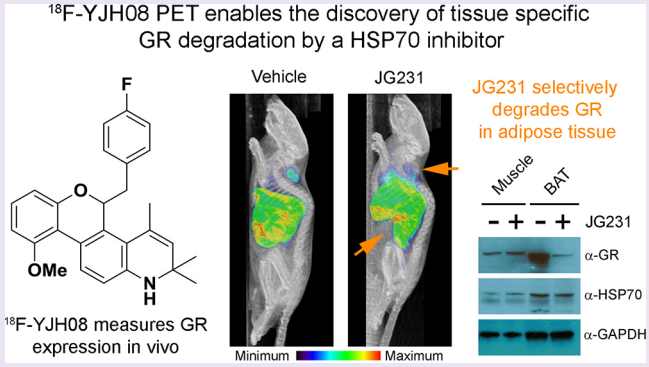

The glucocorticoid receptor (GR) regulates an exceptionally diverse spectrum of physiological processes and is expressed in nearly every normal cell type.[1,2] As a nuclear hormone receptor (NHR), GR regulates biology primarily through an inducible transcriptional mechanism, in which cytosolic corticosteroid agonists bind the isoform GRα to trigger a conformational change that encourages nuclear translocation, homodimerization, and DNA binding to regulate transcription. Agonist bound GRα can also regulate transcription through alternate mechanisms (e.g., tethering other transcription factors to DNA) or through nongenomic signaling. Moreover, other less abundant isoforms of GR, most notably the splice variant GRβ, may regulate additional dimensions of biology in a corticosteroid independent fashion. Further adding to the complexity, GR engages in both cell intrinsic and multiorgan endocrine signaling through secreted hormones (e.g., the hypothalamus−pituitary−adrenal axis).

Because of its seminal importance to the homeostasis of diverse cell types, dysregulation of GR signaling is accompanied by significant, and often highly debilitating, phenotypic changes. For instance, excess or deficient corticosteroid production and the concomitant dysregulation of cellular GRα activity lead to Cushing syndrome or Addison's disease, respectively. Moreover, tissue changes in GR expression—either losses or gains—have been implicated in the pathobiology of a wide spectrum of maladies, including mood disorders, glomerular diseases, and more recently, cancers.[3]

Received: December 27, 2019
Accepted: April 7, 2020
Published: April 7, 2020

https://dx.doi.org/10.1021/acschembio.9b01043
ACS Chem. Biol. 2020, 15, 1381−1391

Cell and genetically engineered animal models have been the mainstays for carefully articulating the above-mentioned features of GR (patho)biology. Fully understanding GR's role in human physiology and disease, as well as developing next generation therapeutics to more selectively modulate GR, requires new technologies that can safely probe GR signaling in living subjects. The lack of noninvasive biomarkers to interrogate GR signaling in humans has left the field to perform very suboptimal assays, for instance, analysis of GR and target gene expression levels from tissues collected at autopsy.[4,5]

With these considerations in mind, we hypothesized that direct measurement of GR expression levels in tissues with nuclear imaging could be an impactful starting point toward developing a complete repertoire of noninvasive tools to study the GR signaling axis. Radiolabeled steroid agonists targeting other NHRs in the same family have been implemented clinically with great success,[6,7] which motivated us to design a radiolabeled small molecule probe targeting the ligand binding domain (LBD) of GR.

Herein, we describe the design, synthesis, and pharmacological evaluation of ^{18}F-5-(4-fluorobenzyl)-10-methoxy-2,2,4-trimethyl-2,5-dihydro-1H-chromeno[3,4-*f*]quinoline (^{18}F-YJH08), a small molecule radiotracer that measures GR expression levels *in vivo* with PET. YJH08 is a potent ligand for GR with weak agonist activity. A high yielding radiosynthesis of ^{18}F-YJH08 was achieved using Cu(II) mediated fluorination of an arylboronic acid pinacol ester precursor. ^{18}F-YJH08 specifically bound to GR in many normal mouse tissues *in vivo*, including several of great interest to the GR signaling community, including the brain, adipose tissue, and adrenals. Lastly, ^{18}F-YJH08 PET was applied to study the anti-GR effects of the bioavailable HSP70 inhibitor JG231. Remarkably, GR degradation only occurred in adipose tissue. This unexpected finding underscores how ^{18}F-YJH08 might be applied to identify tissue specific GR modulators early in the drug discovery process, an important unmet clinical need owing to the intense side effects associated with broad spectrum GR modulators (*e.g.*, the semisynthetic corticosteroid dexamethasone).

RESULTS AND DISCUSSION

Design, Synthesis, and *in Vitro* Characterization of YJH08. The abundance of literature reporting suboptimal imaging findings with radiolabeled corticosteroids suggested to us that we ought to consider nonsteroidal structures with superior pharmacokinetics.[8,9] Agonists generally bind to NHRs with higher affinity compared to antagonists, and highly potent and specific synthetic agonists built on benzopyrano[3,4-*f*]quinolines (Figure 1) were previously shown to be pharmacologically active and well tolerated in animals.[10,11] Therefore, we chose to design a radioligand for GR based on this structural motif.

Prior medicinal chemistry has shown that the C5 position on the benzopyrano[3,4-*f*]quinoline scaffold can tolerate modification without diminishing potency and selectivity for GR, whereas the C10 position is less accepting of manipulation.[12,13] On this basis, we envisioned installing a fluorine atom on the C5 position of the core scaffold. Since ^{18}F-alkyl fluorides can rapidly radio-defluorinate *in vivo*, which results in high bone uptake of the fluoride anion, we chose to couple fluorine to an aromatic ring, a more metabolically stable approach. Retrosynthetically, we anticipated that fluorine-18 could be introduced on the aryl ring through one of several reported copper mediated radiofluorination chemistries.[14,15]

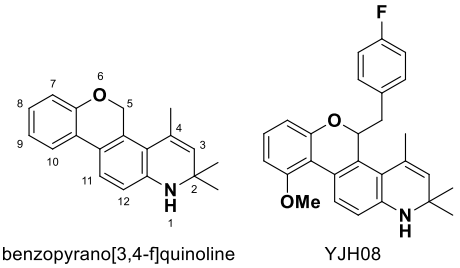

Figure 1. Structure and numbering of the benzopyrano[3,4-*f*]quinoline and the structure of F-5-(4-fluorobenzyl)-10-methoxy-2,2,4-trimethyl-2,5-dihydro-1H-chromeno[3,4-*f*]quinoline (YJH08).

The synthesis of YJH08 began by preparing the methyl acetal **1** in six steps following literature precedent (Scheme 1, see also Supporting Information Methods).[16] To avoid undesired oxidative side products during fluorination chemistry, the secondary amine on the benzopyrano[3,4-*f*]quinoline scaffold was protected with Boc_2O to confer **2**. A Grignard reaction with 4-bromobenzylmagnesium bromide was applied to install an aromatic moiety on the C5 position (**3**). A Stille-type coupling was then invoked to convert the aryl bromide to an arylboronic acid pinacol ester (**4**). This functional group was desired as it has been successfully used as a substrate for regioselective copper mediated radiofluorination reactions.[17,18] Satisfyingly, we were able to convert this molecule to the aryl fluoride **5** at 68% yield within 2 h at 120 °C using $Cu(OTf)_2(Py)_4$, pyridine, KF, and $K_{2.2.2}$. The Boc group was then efficiently removed in 30 min with 50% TFA in DCM to confer **6**. In summary, the overall yield of **4** was 25%, and the yield of **6** was 15%.

Next, the affinity of YJH08 for GR and the other type 1 subfamily 3 nuclear hormone receptors was evaluated using ^{3}H-ligand displacement assays on cells. The K_i of YJH08 for GR was determined to be ∼0.4 nM, or about 10-fold more potent than the agonist dexamethasone (Table 1 and Figure 2A). Moreover, YJH08 bound to GR with at least 100 fold higher relative affinity than other type 1 subfamily 3 nuclear hormone receptors (Table S1 and Figure S1). We conducted cell-based studies to determine if YJH08 modulates GR activity. Real time PCR showed that YJH08 (10 μM, 6 h exposure) elevated the levels of two GR target genes (GILZ, FKBP5) in DU145, a GR positive human prostate cancer cell line (Figure 2B). The induction per gene was lower than what was observed for dexamethasone (1 μM, 6 h exposure), and one gene, Per1, was induced by dexamethasone but not YJH08. Overall, these data suggest that YJH08 may be a mild GR agonist.

Radiosynthesis of ^{18}F-YJH08. A focused screen of reaction conditions revealed that ^{18}F-Boc-YJH08 could be efficiently synthesized by hand in 20 min using K_2CO_3/KOTf as the base to mobilize ^{18}F-fluoride anions from a QMA column (4.7 ± 0.8%, see Table S2, Figure S2, and Scheme 2). We also found that this reaction was amenable to automation using an ELIXYS FLEX/CHEM synthesis module, and HPLC analysis of the reaction progress showed that the reaction produces one major radioactive peak corresponding to ^{18}F-Boc-YJH08 (Figure 3A). After purification, the Boc protecting group was removed with 50% TFA in DCM to confer ^{18}F-YJH08 in 12.4 ± 3% decay corrected radiochemical yield (Figure 3B and Figure S3). The molar activity of ^{18}F-YJH08 was calculated to be 0.042 ± 1 Ci/μmol over four independent radiosyntheses (Figure S4). The partition coefficient (log *P*) of ^{18}F-YJH08 was assessed in instant thin layer chromatography and calculated to be 2.78.

https://dx.doi.org/10.1021/acschembio.9b01043
ACS Chem. Biol. 2020, 15, 1381−1391

Scheme 1. Synthesis of YJH08[a]

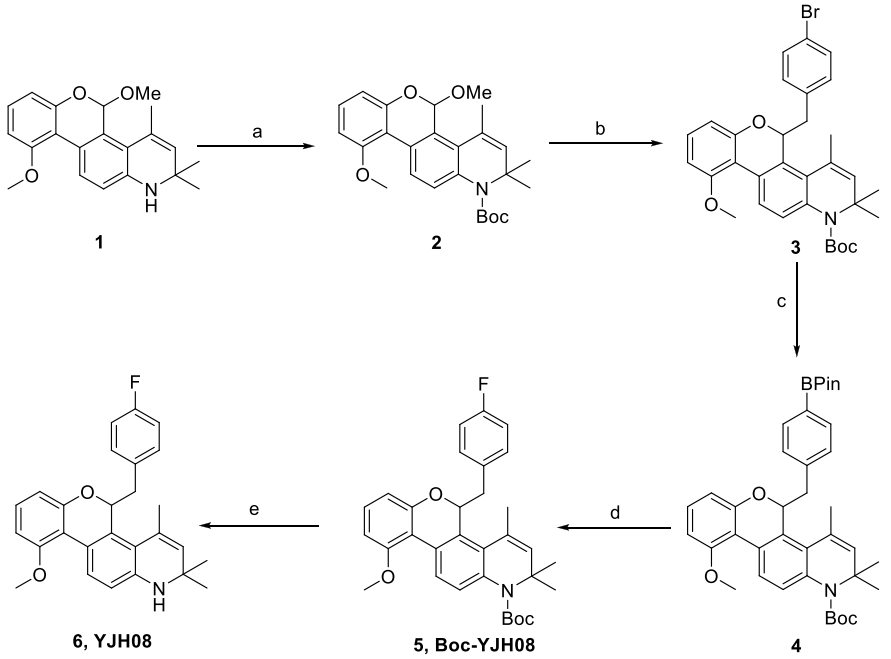

[a]Reagents and conditions: (a) *n*-BuLi, $(Boc)_2O$, THF, −45 °C, 51%; (b) 0.25 M 4-Bromobenzylmagnesium bromide in anhydrous Et_2O, BF_3·Et_2O, anhydrous DCM, −15 °C, 73%; (c) Pd(dppf)Cl_2·DCM, KOAc, B_2Pin_2, anhydrous dioxane, 100 °C, 68%; (d) $Cu(OTf)_2(Py)_4$, Py, KF, K_{222}, DMF, 120 °C, 68%; (e) 50% TFA in CH_2Cl_2, 40 °C, 30 min, 95%.

Table 1. A Summary of the Binding Affinity of YJH08 Compared to Conventional Agonists for Subfamily 3 Nuclear Hormone Receptors[a]

	K_i (M)				
ligand	GR	AR	PR	ER	MR
reference[b]	2.03×10^{-9}	4.96×10^{-10}	6.27×10^{-10}	6.94×10^{-9}	1.41×10^{-8}
YJH08	4.01×10^{-10}	2.20×10^{-7}	5.55×10^{-7}	1.90×10^{-5}	2.90×10^{-7}

[a]The competitive binding data are presented in Figure 2A and Figure S2. The data were fit using a one site K_i and nonlinear regression with Prism software. The data are representative of two independent experiments. [b]Reference ligands were dexamethasone (GR), dihydrotestosterone (AR), progesterone (PR), estradiol (ER), and aldosterone (MR). Abbreviations: GR = glucocorticoid receptor, AR = androgen receptor, PR = progesterone receptor, ER = estrogen receptor, MR = mineralocorticoid receptor.

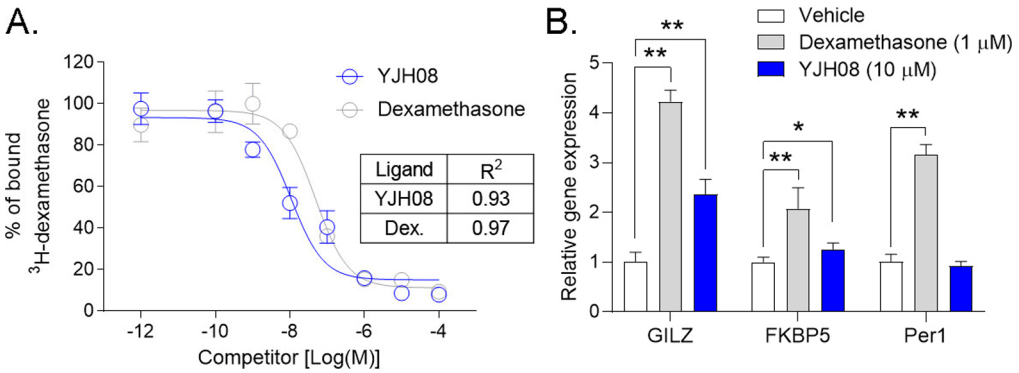

Figure 2. YJH08 is a high affinity ligand for GR with weak agonist properties. (A) A ligand displacement curve showing YJH08 and dexamethasone displace ^{3}H-dexamethasone in DU145 cells. The data were fit using a one site nonlinear regression, and the coefficient of determination (R^2) values are highlighted in the inset box. Additional competitive binding curves are presented in the Supporting Information. (B) Real time PCR data showing the relative induction of three GR target genes in DU145 cells by dexamethasone (1 μM) or YJH08 (10 μM). Cells were harvested for mRNA analysis after a 6 h exposure to drug or vehicle. The data, normalized to the ΔCt levels in vehicle treated cells, support an assessment that YJH08 may be a weaker GR agonist than dexamethasone. Statistical significance was assessed using an unpaired, two-sided Student's *t* test. $^{**}P < 0.01$, $^{*}P < 0.05$.

https://dx.doi.org/10.1021/acschembio.9b01043
ACS Chem. Biol. 2020, 15, 1381−1391

Scheme 2. Radiosynthesis of ^{18}F-YJH08

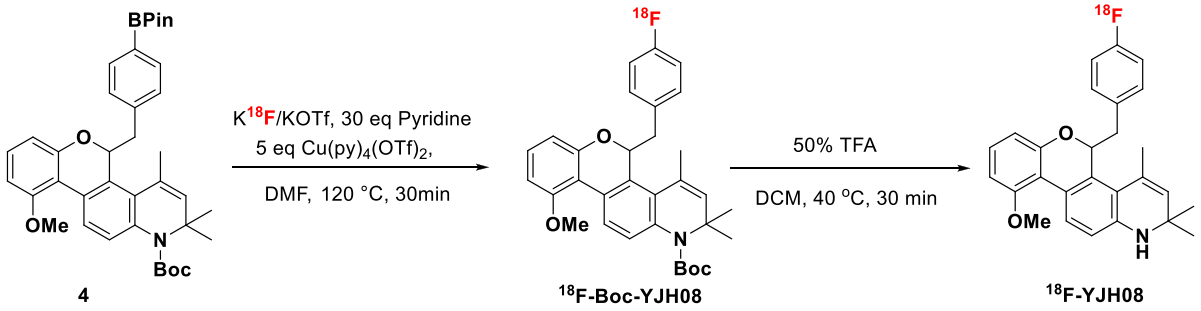

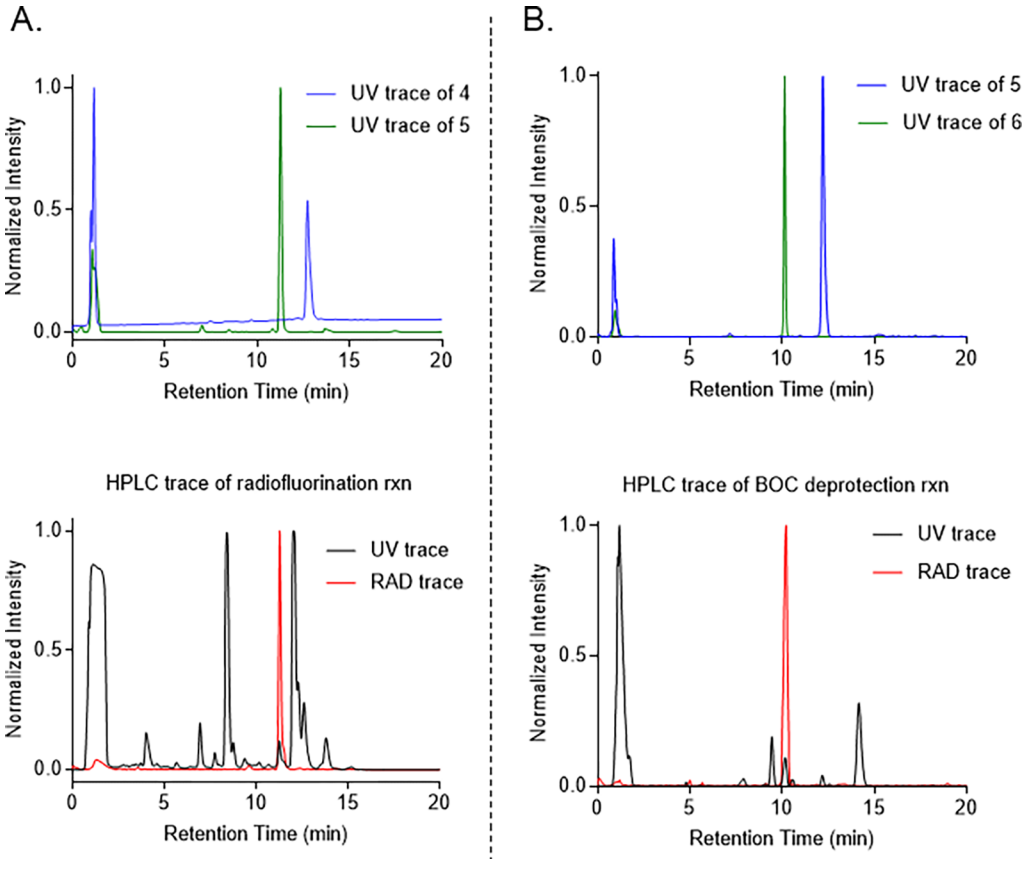

Figure 3. (A) Stacked semipreparative UV HPLC traces showing the retention of arylboronic acid pinacol ester starting material (**4**) and the Boc-protected aryl fluoride product (**5**). Below these analytical standards are shown the UV trace of the complex reaction mixture at 90 min and the corresponding trace collected using a radiation detector. A single product peak is observed in RAD-HPLC corresponding to the desired product, ^{18}F-**5**, while a minor UV peak is observed at the same retention time, as desired. The peak was collected and transferred immediately to a reaction vial for Boc deprotection. (B) Stacked semipreparative UV HPLC traces showing the retention of the Boc protected aryl fluoride (**5**) and the deprotected final product (**6**). Below the analytical standards are shown the UV trace of the complex reaction mixture at 30 min and the corresponding trace collected using a radiation detector. A single product peak is observed in RAD-HPLC corresponding to the desired product, ^{18}F-YJH08, while a minor UV peak is observed at the same retention time, as expected. After purification, the purity and identity of ^{18}F-YJH08 were confirmed using analytical HPLC with an isocratic gradient.

^{18}F-YJH08 Specifically Binds GR *in Vivo* and Measures Receptor Saturation by a Synthetic GR Agonist. To understand the biodistribution of ^{18}F-YJH08 *in vivo*, we first conducted a dynamic PET scan over 60 min in immunocompetent intact male C57Bl6/J mice. Region of interest analysis was applied to generate time activity curves, which revealed several enlightening trends (Figure 4A,B and Figure S5). First, the radiotracer rapidly cleared from serum, and fitting the data with a two phase exponential decay curve estimated the fast and slow half-lives to be ∼21 s and ∼760 s, respectively. Moreover, liver uptake was prominent at very early time points post injection (0−300 s), with continuous washout from ∼300 to 3600 s. These data suggest a hepatobiliary mechanism of clearance. Consistent with this model, significantly lower radiotracer accumulation was observed in the kidneys from 0 to 3600 s. Radiotracer uptake in the bone was low and approximately equivalent to muscle, which suggests that the compound is stable to radiodefluorination *in vivo*.

Notably, we also observed clear radiotracer uptake in tissues for which aberrant GR expression is thought to drive disease

https://dx.doi.org/10.1021/acschembio.9b01043
ACS Chem. Biol. 2020, 15, 1381−1391

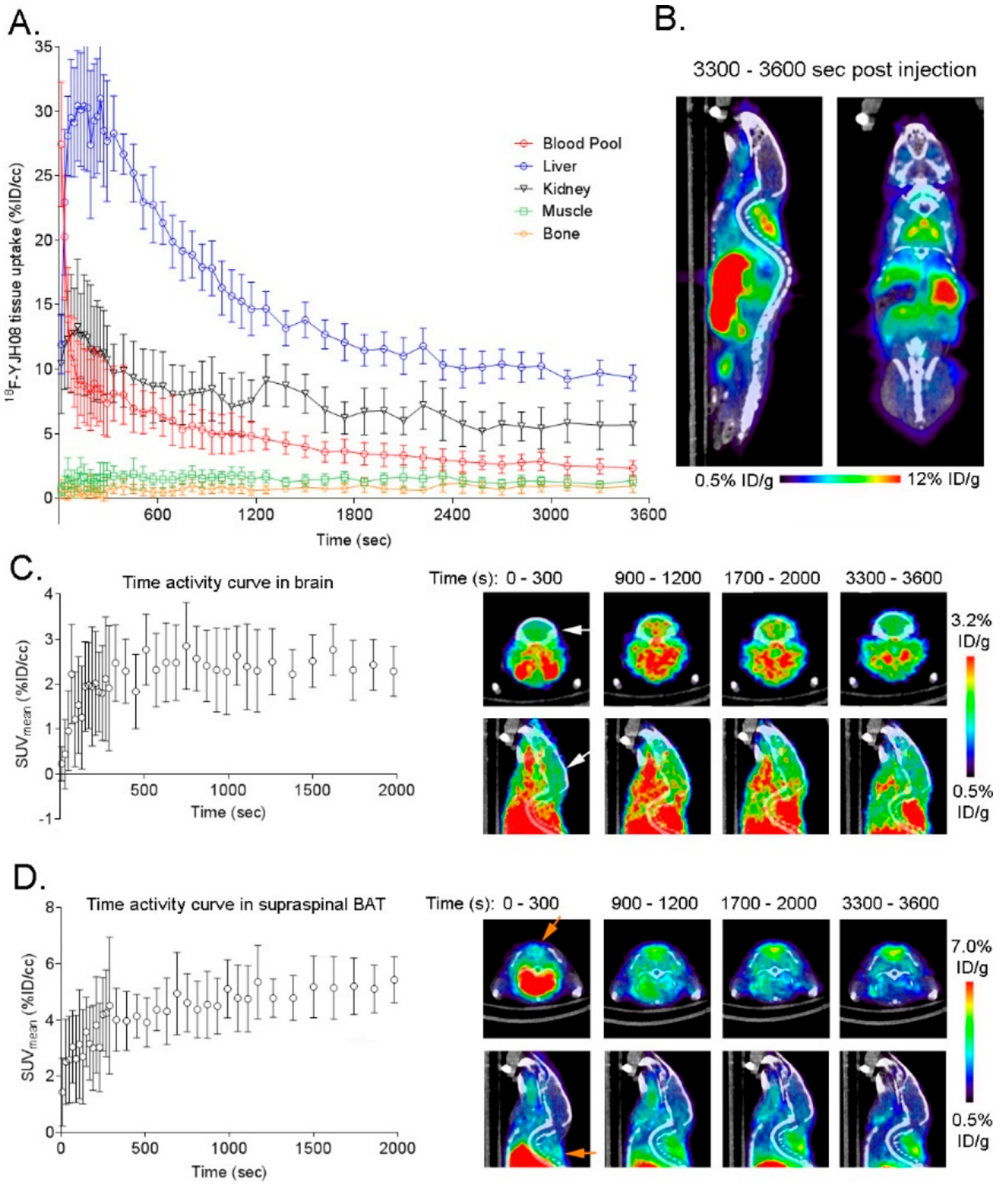

Figure 4. ^{18}F-YJH08 accumulates in GR rich tissues important to normal and disease physiology, including the brain. (A) A time activity curve from a dynamic PET scan shows the magnitude of radiotracer uptake and clearance in major tissue compartments of a male C57Bl6/J mouse. The radiotracer rapidly targeted the liver within 200 s post injection, with continuous washout from 300−3000 s, suggesting a hepatobiliary clearance mechanism. An early increase and washout in kidney uptake was followed by stable accumulation. Muscle and bone uptake were significantly lower than liver and kidney. (B) Representative sagittal and coronal slices of the mouse used to derive the time activity curves provide a visual rendering of relative radiotracer biodistribution in tissues. (C) Region of interest analysis performed on the PET data from the dynamic acquisition shows high and time dependent radiotracer accumulation in the brain. At right are shown representative transaxial and sagittal images centered on the mouse brain (arrow) to highlight the uptake of the radiotracer over time. (D) Region of interest analysis on the supraspinal brown adipose tissue depot was used to calculate the depicted time activity curve. The magnitude of radiotracer uptake was statistically higher that muscle and bone from ∼300 to 3600 s post injection. At right are shown representative transaxial and sagittal images centered on the supraspinal pad of brown adipose tissue. Images from the indicated time intervals are shown to depict the accumulation of the radiotracer over time. Washout of the radiotracer from the blood pool can also be observed in the transaxial view.

pathobiology. For instance, we observed high radiotracer uptake in the brain (Figure 4C), a significant finding as the neuroimaging community has long sought to develop a noninvasive tool to measure changes in GR expression thought to be occurring in the brains of individuals suffering from mood disorders (e.g., anxiety, depression).[19] Moreover, high tracer uptake occurred in supraspinal brown adipose tissue in which GR expression is expressed and hypothesized to regulate seminal processes like thermogenesis and beiging (Figure 4D).[20] Last, we performed a broader survey of radiotracer biodistribution by analyzing tissues post mortem. In general, numerous GR rich tissues had high radiotracer uptake, including the adrenals, lungs, and heart (Table 2).

We next tested if ^{18}F-YJH08 accumulation in tissues is due to specific GR binding. First, biodistribution studies were conducted to determine if dexamethasone treatment lowered ^{18}F-YJH08 uptake in normal mouse tissues due to competitive GR binding. Previous studies, including our own experience with a radiofluorinated corticosteroid termed ^{18}F-GR02, have shown that it can be challenging to engage GR with a

https://dx.doi.org/10.1021/acschembio.9b01043
ACS Chem. Biol. 2020, 15, 1381−1391

Table 2. Biodistribution Data Collected 30, 60, 90 min after Injection of ^{18}F-YJH08 in C57Bl6/J Mice[a]

Tissue	30 min	60 min	90 min
blood	0.85 ± 0.1	0.57 ± 0.02	0.49 ± 0.06
brain	1.68 ± 0.14	1.33 ± 0.06	0.97 ± 0.03
heart	3.04 ± 0.75	1.33 ± 0.21	0.92 ± 0.14
lung	2.65 ± 0.19	2.02 ± 0.29	1.39 ± 0.1
liver	11.03 ± 0.89	7.7 ± 0.69	8.43 ± 1.38
spleen	1.59 ± 0.13	0.83 ± 0.02	0.74 ± 0.15
pancreas	4.5 ± 0.15	2.63 ± 0.05	1.9 ± 0.41
kidney	4.5 ± 0.5	2.35 ± 0.34	1.86 ± 0.26
stomach	1.88 ± 0.96	1.63 ± 0.92	2.61 ± 1.54
small intestine	19.05 ± 3.27	8.61 ± 2.68	7.67 ± 2.34
large intestine	1.33 ± 0.35	1.23 ± 0.43	6.67 ± 4.73
supraspinal BAT	14.41 ± 3.42	16.4 ± 4.93	14.58 ± 1.91
muscle	1.49 ± 0.2	1.15 ± 0.03	0.85 ± 0.18
bone	1.11 ± 0.15	0.61 ± 0.15	0.58 ± 0.16
adrenal gland	20.02 ± 2.21	9.43 ± 0.08	5.72 ± 2.32

[a]The data are represented as mean ± standard deviation of the % ID/g.

cointravenous injection of excess cold ligand to an extent that measurably alters tracer biodistribution in tissues.[9] We proposed that the solubility limits of hydrophobic steroids and steroid-like molecules in intravenous formulations account for this observation, as we also found that administering a competitive ligand for GR *via* gavage hours to days in advance of the imaging study very effectively suppressed radiotracer uptake. With this experience in mind, we administered dexamethasone *via* oral gavage in two ways. One treatment arm of C57Bl6/J mice received dexamethasone once (50 mg/kg) at 4 h prior to ^{18}F-YJH08 injection, and another cohort received the drug once daily (100 mg/kg) *via* oral gavage for 3 days prior to the radiotracer injection. Biodistribution studies showed that a single dose of dexamethasone reduced radiotracer uptake in the small intestine, while a higher dose administered over several days suppressed radiotracer uptake in many tissues compared to mice receiving vehicle (Figure 5A and Figures S6, S7). To confirm that high dose dexamethasone did not unexpectedly reduce GR expression levels, we examined GR expression in select tissues in which a significant degree of radiotracer suppression was observed. We found that GR expression levels were equivalent in several normal tissues from treated and untreated mice, which provides confidence that the suppression of radiotracer uptake was due to competitive GR binding (Figure S8). We next evaluated radiotracer uptake in adrenalectomized (adx) mice, as disruption of the HPA axis is well understood to ablate circulating corticosteroids while triggering normal cells to autonomously upregulate GR. ^{18}F-YJH08 uptake was higher in the tissues of adx mice compared to intact mice (Figure 5A and Figure S9). Collectively, these data show that tissue uptake of the radiotracer is a reflection of GR abundance and occupancy by endogenous ligand.

On PET, visually obvious decreases in radiotracer uptake due to dexamethasone treatment (100 mg/kg) were observed in several tissues (e.g., brain, supraspinal brown adipose tissue, and kidneys, see Figure 5B). Moreover, digital autoradiography was applied to compare the intensity of radiotracer binding in the brain sections from adx mice to those from intact mice treated with dexamethasone (Figure 5C). Comparison of the relative intensity of the pseudocolor showed that radiotracer binding was uniformly higher in adx mice, as expected. Radiotracer binding was high in the isocortex, a relatively large anatomical area known to have high GR expression in the mouse brain based on *in situ* hybridization data (Figure S10). GR is highly expressed in smaller structures within the brain, for example the hippocampal formation, although this was challenging to detect with the limited resolution of autoradiography. Studies in nonhuman primates or humans will be required the interrogaion of the regions of specific GR binding within complex organs like the brain.

Finally, we conducted an exploratory study to determine if genetic knockout of GR reduced ^{18}F-YJH08 uptake. Mice bearing *loxP* sites flanking exon 3 of the *Nr3cl* gene were crossed with mice bearing Cre recombinase under the control of the adiponectin promoter to induce adipocyte specific GR knockout. PET/CT data clearly showed that ^{18}F-YJH08 uptake was significantly reduced in several fat depots within the $GR^{fl/fl}$, *Adipoq-Cre* knockout mice, most obviously the supraspinal and scapular brown fat depots (Figure 5D). Moreover, overall radiotracer binding in the abdomen was significantly reduced in the knockout mice compared to wild type litter mate control, which is likely attributable to a loss of GR in fat depots as well as the greater omentum. To our knowledge, this is the first reported evidence of specific radioligand binding to GR in the adipose tissue.

^{18}F-YJH08 Reveals Tissue Specific Modulation of GR Expression by JG231, a Potent HSP70 Inhibitor. The limitations of broad-spectrum GR modulators like corticosteroids are well-known, and the severe side effects associated with their long-term use (e.g., diabetes mellitus, osteoporosis) motivated drug development campaigns starting in the 1990s to identify safer GR modulators that selectively modulate GR activity.[21] We hypothesized that ^{18}F-YJH08 PET could complement these ongoing efforts by revealing tissue specific drug−GR interactions. To test this concept, we evaluated the biodistribution of ^{18}F-YJH08 in mice after treatment with JG231, a potent HSP70 inhibitor that we have shown can induce GR degradation (Figure 6A and B).[22] JG231 has a well-defined pharmacokinetic profile, and our prior experience with this molecule showed it to have antitumor activity in prostate cancer mouse models.[23] Using the same treatment strategy, mice were subjected to 4 mg/kg/day for 3 days intraperitoneally and subsequently treated with ^{18}F-YJH08. On PET, the only visually obvious alterations in radiotracer distribution were noted in the supraspinal brown fat depot and in a portion of the abdomen that we interpreted to be the greater omentum (Figure 6C). In these regions, it appeared that JG231 suppressed radiotracer binding, perhaps indicative of GR degradation. Post mortem imaging of the supraspinal brown fat depot more clearly showed that JG231 dramatically reduced ratiotracer binding compared to the same tissue harvested from mice treated with vehicle (Figure 6C). Biodistribution studies also suggested that JG231 most significantly induced GR degradation in brown fat (Figure 6D). Immunoblot studies corroborated the biodistribution data, showing approximately ∼50% reduction in GR expression levels due to JG231 treatment in brown fat, and no change in GR levels from other tissues, for example, kidneys, liver, and muscle (Figure 6E and Figure S11). To our knowledge, this is first example of tissue specific GR degradation. More generally, these early data suggest that ^{18}F-YJH08 PET could be applied to identify therapies with unexpected tissue tropism or prospectively engineer desirable tissue specificity into experimental GR modulators.

https://dx.doi.org/10.1021/acschembio.9b01043
ACS Chem. Biol. 2020, 15, 1381−1391

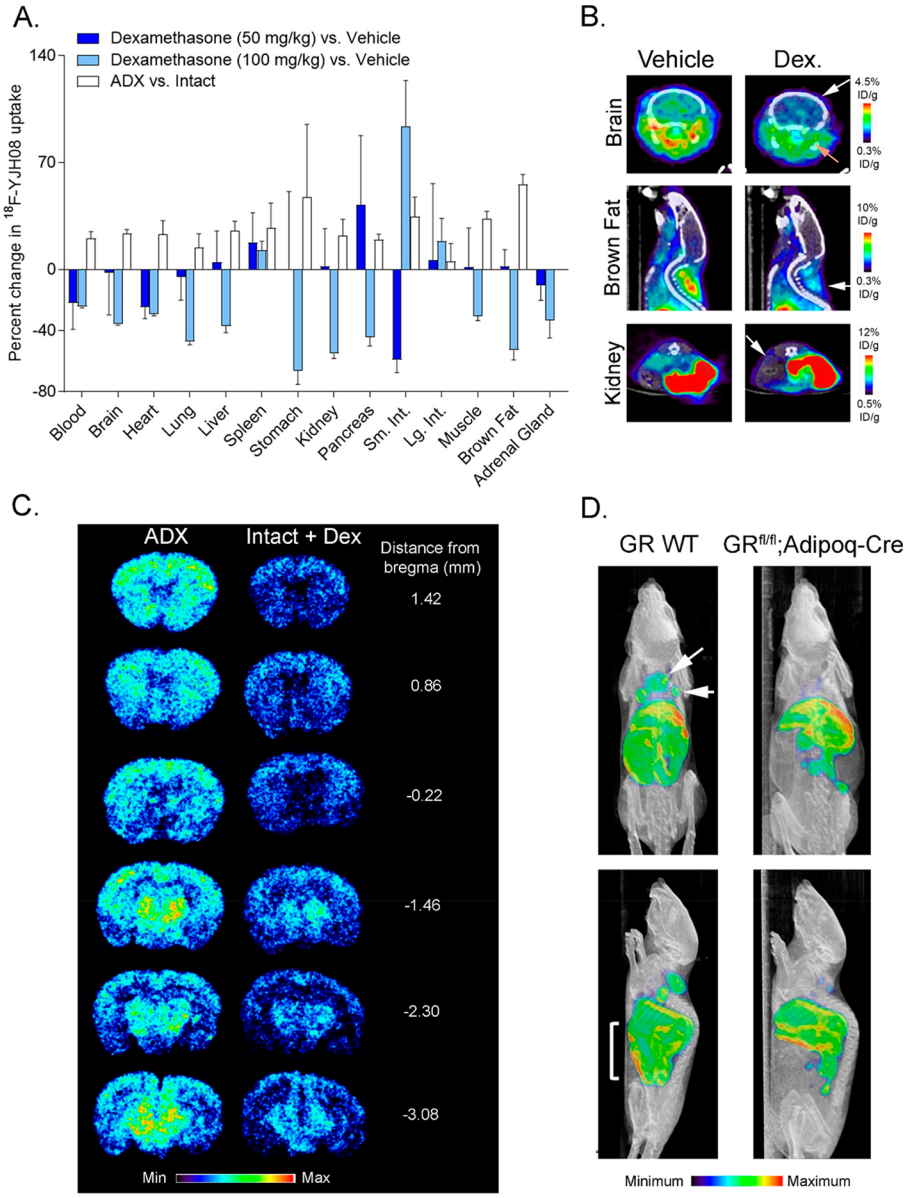

Figure 5. ^{18}F-YJH08 specific binding to GR *in vivo* and application to measure receptor occupancy by endogenous or exogenous ligands. (A) A summary of the percent change in radiotracer uptake for mouse tissues in three separate cohorts comparing (1) the impact of dexamethasone treatment at 50 mg/kg *via* gavage 4 h before the radiotracer injection, (2) the impact of dexamethasone treatment at 100 mg/kg/day *via* gavage 3 days before the radiotracer injection, and (3) the impact of adrenalectomy (adx.) on ^{18}F-YJH08 tissue biodistribution. (B) Representative PET/CT slices showing the suppression of radiotracer uptake due to prior dexamethasone treatment in the brain (top white arrow), supraspinal brown fat (middle white arrow), and the kidneys (bottom white arrow). A tan arrow was placed over a submandibular region that showed evidence of specific binding that could represent anterior cervical or supraclavicular brown fat. These data were taken from the cohort that received 100 mg/kg/day. (C) Digital autoradiography showing the relative radiotracer binding in coronal sections of the brains of mice from adx mice or intact mice treated with dexamethasone. (D) Maximum intensity projections showing the distribution of ^{18}F-YJH08 in wild type female C57Bl6/J mice and a female littermate with adipocyte specific GR knockout. White arrows are positioned on the supraspinal brown fat depot and the bilateral scapular brown fat depots on the transverse view of the wild type mouse. A white bracket is positioned over the region of the abdomen expected to be encompassed by the omentum on the sagittal view of the wild type mouse. Radiotracer uptake is absent in all highlighted regions in the *GR$^{fl/fl}$, Adipoq-Cre* mouse.

CONCLUSIONS

Here, we report the design, synthesis, and characterization of ^{18}F-YJH08, a first in class radioligand to measure GR expression noninvasively with PET. *In vivo* studies showed that ^{18}F-YJH08 specifically binds to virtually all normal tissues in mice, including tissue compartments like the brain for which the imaging community has long desired biomarkers to study the GR signaling axis. Moreover, the level of GR specific binding in tissues observed with ^{18}F-YJH08 stands out compared to previously reported biodistribution data for radiotracers targeting GR, including nonsteroidal agonists.[24] We further show the radiotracer can be used to study the pharmacology of GR modulators, which led to the unexpected finding of tissue specific anti-GR activity for an inhibitor of HSP70, a protein expressed in virtually every tissue in the body. Overall, ^{18}F-YJH08 provides an unprecedented multiorgan view of GR expression in real time, and its clinical translation will likely open

https://dx.doi.org/10.1021/acschembio.9b01043
ACS Chem. Biol. 2020, 15, 1381−1391

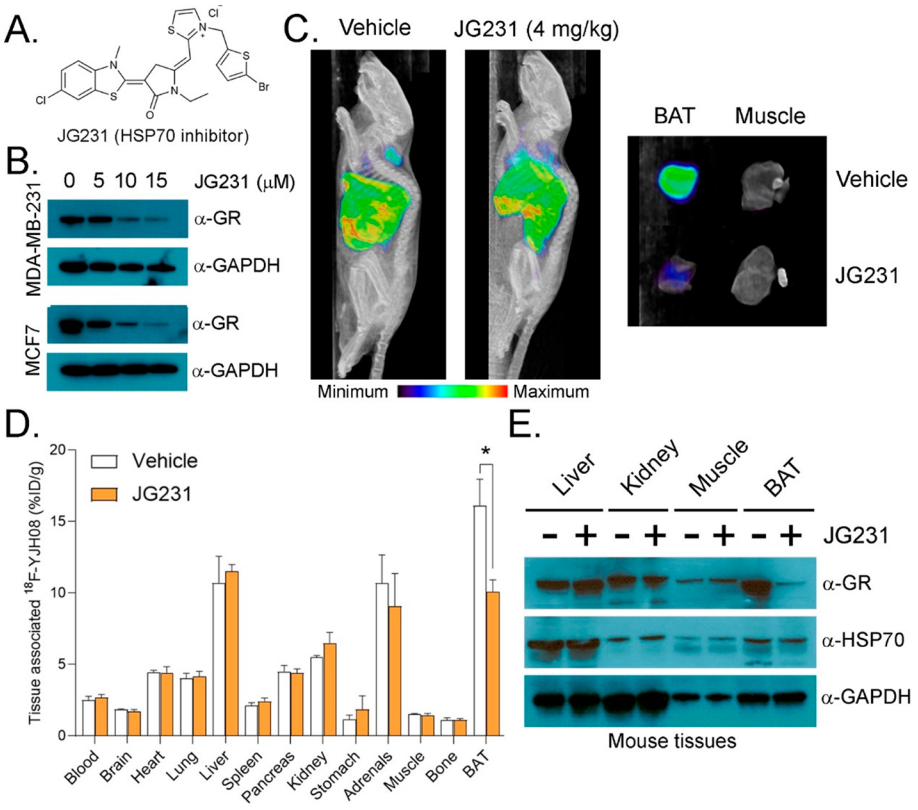

Figure 6. ^{18}F-YJH08 revealing unexpected tissue specific GR degradation for an HSP70 inhibitor. (A) The structure of JG231, a recently developed potent HSP70 inhibitor with excellent pharmacokinetics and antitumor activity. (B) Immunoblot data showing that JG231 degrades GR in MCF7 and MDA MB 231, two human breast cancer cell lines. Cells were treated with the indicated dose for 24 h. (C) Maximum intensity projections of viable mice showing the suppression of radiotracer uptake by JG231 treatment in the supraspinal brown fat depot and the omentum, but not in other tissues with high radiotracer uptake. At right is shown a maximum intensity projection of supraspinal BAT and muscle from a representative mouse in either treatment arm. Mice (n = 5/treatment arm) were treated with JG231 or vehicle once daily for 3 days *via* intraperitoneal injection. (D) Biodistribution data showing the tissue uptake of ^{18}F-YJH08 in mice from the treatment study. As predicted by the PET/CT data, JG231 suppressed radiotracer uptake exclusively in the supraspinal brown fat pad. *P < 0.01. The biodistribution data are representative of two independent experiments. (E) Immunoblot data showing GR degradation in brown fat after treatment with JG231. GR levels were not impacted in liver, kidneys, or muscle, as predicted based on the radiotracer biodistribution data.

new frontiers in our understanding of the (patho)biology of GR in humans.

EXPERIMENTAL SECTION

Radiosynthesis of ^{18}F-YJH08. To identify optimal conditions for radiofluorination, the following workflow was applied by hand. An aqueous solution of H^{18}F (20 mCi) was passed through a Sep-Pak light QMA cartridge, which was previously activated with distilled water (3 mL). A ^{18}F fluoride ion was eluted with 0.5 mL of a K_2CO_3/KOTf solution (0.1 mg mL^{-1} and 6 mg mL^{-1} in 1:1 CH_3CN/H_2O). The solution was dried at 110 °C under a gentle stream of argon gas and then azeotropically dried twice with anhydrous acetonitrile (1 mL) at 110 °C under a gentle stream of argon. To the reaction vial containing ^{18}F was added a solution of precursor **4** (2 mg), $Cu(Py)_4(OTf)_2$ (10.9 mg, 5 equiv), and pyridine (8 μL, 30 equiv) in anhydrous DMF (0.5 mL). The mixture was heated to 110 or 120 °C and stirred for 30 min. The reaction was carefully monitored by radio-TLC for conversion.

On an ELIXYS FLEX/CHEM synthesis module (Sofie Biosciences), ^{18}F-Boc-YJH08 was prepared in 90 min and then transferred from the ELIXYS on a C18 Sep-Pak cartridge. The ^{18}F-Boc-YJH08 was eluted from the cartridge using anhydrous CH_3CN and purified by semipreparative HPLC (50% to 95% CH_3CN in water over 12 min and 95% CH_3CN in water for another 8 min) to obtain the desired compound in a decay-corrected radiochemical yield of 12.4 ± 3% (n = 10). The purity of the compound was further verified by reinjection on the semipreparative HPLC.

^{18}F-Boc-YJH08 was dissolved in a 1.0 mL solution of 50% trifluoroacetic acid in CH_2Cl_2, and the reaction was stirred at 40 °C for 30 min to remove the Boc protecting group. After the reaction was complete on TLC, the reaction vial was then cooled to 0 °C and quenched by adding DMF (0.5 mL), followed by the dropwise addition of 5 M NaOH solution (aq, 0.5 mL). The DCM was removed under reduced pressure, and the mixture was subjected to the semipreparative HPLC (30% to 95% CH_3CN in water over 12 min, then 95% CH_3CN for 8 min) for the purification, which provided the radioactive production in a decay-corrected radiochemical yield of 6.7 ± 1% (n = 10). The purity of the compound was further verified by reinjection of pure compound on semipreparative HPLC.

To prepare the radiotracer for animal studies, ^{18}F-YJH08 was trapped on the cartridge and eluted with CH_3CN (1 mL). After removing the organic solvent, the pure product was dissolved in an injection formulation of 1/1/8 (v/v/v) DMSO/Tween 80/Saline. The stability, UV purity, and radiochemical purity of ^{18}F-YJH08 in formulation was further confirmed by analytical HPLC equipped with a gamma ray radio detector and a UV detector at 254 nm. The analytical HPLC condition was as follows: Waters C18 (4.6 mm × 150 mm, 5 μm), mobile phase acetonitrile/H_2O, 8:2 (v/v); flow rate = 1 mL/min. Both the UV and Rad spectrum comigrated with the analytical standard, and the purity of the tracer was ∼97%.

Animal Studies. All animal experiments were conducted under the approval of the Institutional Animal Care and Use Committee (IACUC) at UCSF. Male *nu/nu* or C57BL6/J mice (4–6 weeks) were purchased from Charles River. All the mice were housed in a

https://dx.doi.org/10.1021/acschembio.9b01043
ACS Chem. Biol. 2020, 15, 1381−1391

dedicated vivarium with free access to food and water. For dexamethasone treatment studies, mice were treated *via* oral gavage with vehicle (0.5% hydroxy-propyl-methylcellulose and 0.2% Tween 80 in water) or dexamethasone (100 mg/kg or 50 mg/kg). For JG231 treatment studies, mice were treated *via* intraperitoneal injection of JG231 (4 mg/kg) in injectable formulation (10% DMSO, 18% Tween80, 3.6% dextrose, 68.4% 1 M HEPES) or vehicle. The mice were treated once daily for 3 days. At day 3, the mice received the radiotracer after the final gavage or injection. Adrenalectomized mice were purchased from Charles River and provided drinking water supplemented with NaCl (aq) per instructions until the time of the tracer biodistribution study.

Small Animal PET/CT. Prior to injection, the formulated dose of ^{18}F-YJH08 was passed through a sterile 0.22 μm membrane. Approximately 300 μCi was injected *via* tail vein in a volume of 100−150 μL per mouse. After the indicated period of uptake time, the mice were anesthetized with 2−3% isoflurane and imaged with a Siemens Inveon micro PET/CT. For dynamic acquisitions, the mice were anesthetized prior to injection and injected while positioned on the scanner bed. All imaging data were decay corrected, reconstructed, and analyzed with AMIDE software. Maximum intensity projections (MIPs) were generated by AMIDE software. Regions of interest (ROI) were manually placed to calculate SUV_{mean} data from the dynamic acquisitions.

Biodistribution Studies. Mice were euthanized after radiotracer injection with CO_2 (g) asphyxiation and dissected at dedicated time points post injection. The blood and tissues were removed, washed, dried, and weighed. The activity of each tissue was measured with a gamma counter. All data was decay corrected. PRISM software was used to express a percentage (% ID/g) of the injected dose per gram of tissue.

Autoradiography. Twenty minutes postinjection of ^{18}F-YJH08, mice were anesthetized and were perfused with cold PBS *via* cardiac puncture. Tissues were immediately collected and flash frozen in OCT on dry ice. Tissues were sectioned on a microtome at a thickness of 20 μm and immediately mounted on glass slides. The slides were then exposed on a GE phosphor storage screen, and the screen was developed on an Amersham Typhoon 9400 phosphorimager. H&E staining was performed by the Pathology Core Facility at UCSF. The autoradiography images were processed using ImageJ software.

Generation of the Transgenic Mice with Adipocyte Specific GR Knockout. To generate mice with *Nr3c1* selectively deleted in mature adipocytes, female GR floxed mice (Jackson Laboratory, cat. no. 021021) were crossed to a male mouse carrying a transgene that expresses the Cre recombinase enzyme (Cre) under the regulation of the adiponectin promoter and enhancer elements (Jackson Laboratory, cat. no. 028020). This adiponectin-Cre (adipo-Cre) mouse line has been validated by a number of laboratories to selectively express Cre in mature adipocytes.[25] Progeny from this cross with both adipo-Cre and floxed *Nr3c1* had the *Nr3c1* gene deleted in their adipocytes.[26] Knockout mice from this cross are born in normal Mendelian ratios and have no obvious health issues.

Statistics. All statistical analysis was performed using PRISM v6.0 software. An unpaired, two-tailed Student's *t* test was used to determine statistically significant differences in the data. Changes at the 95% confidence level ($P < 0.05$) were reported as statistically significant. For the determination of K_i, the data were fit with a one site nonlinear regression model.

■ ASSOCIATED CONTENT

Supporting Information

The Supporting Information is available free of charge at https://pubs.acs.org/doi/10.1021/acschembio.9b01043.

Additional experimental details, figures, and schemes (PDF)

■ AUTHOR INFORMATION

Corresponding Author

Michael J. Evans − *Department of Radiology and Biomedical Imaging, Helen Diller Family Comprehensive Cancer Center, and Department of Pharmaceutical Chemistry, University of California, San Francisco, San Francisco, California 94158, United States;* orcid.org/0000-0003-4947-1316; Phone: 415-514-1292; Email: michael.evans@ucsf.edu; Fax: 415-353-9425

Authors

Yangjie Huang − *Department of Radiology and Biomedical Imaging, University of California, San Francisco, San Francisco, California 94158, United States*

Ning Zhao − *Department of Radiology and Biomedical Imaging, University of California, San Francisco, San Francisco, California 94158, United States;* orcid.org/0000-0003-3699-3369

Yung-hua Wang − *Department of Radiology and Biomedical Imaging, University of California, San Francisco, San Francisco, California 94158, United States*

Charles Truillet − *Imagerie Moleculaire in Vivo, INSERM, CEA, Universitée Paris Sud, CNRS, Universite Paris Saclay, CEA-Service Hospitalier Frederic Joliot, Orsay 94100, France*

Junnian Wei − *Department of Radiology and Biomedical Imaging, University of California, San Francisco, San Francisco, California 94158, United States*

Joseph E. Blecha − *Department of Radiology and Biomedical Imaging, University of California, San Francisco, San Francisco, California 94158, United States*

Henry F. VanBrocklin − *Department of Radiology and Biomedical Imaging and Helen Diller Family Comprehensive Cancer Center, University of California, San Francisco, San Francisco, California 94158, United States*

Youngho Seo − *Department of Radiology and Biomedical Imaging and Helen Diller Family Comprehensive Cancer Center, University of California, San Francisco, San Francisco, California 94158, United States*

Mohd Sayeed − *Department of Pediatrics, University of California San Francisco, San Francisco, California 94158, United States*

Brian J. Feldman − *Department of Pediatrics, University of California San Francisco, San Francisco, California 94158, United States*

Rahul Aggarwal − *Helen Diller Family Comprehensive Cancer Center, University of California, San Francisco, San Francisco, California 94158, United States; Department of Medicine, Division of Hematology/Oncology, University of California San Francisco, San Francisco, California 94158, United States*

Spencer C. Behr − *Department of Radiology and Biomedical Imaging and Helen Diller Family Comprehensive Cancer Center, University of California, San Francisco, San Francisco, California 94158, United States*

Hao Shao − *Department of Pharmaceutical Chemistry, University of California, San Francisco, San Francisco, California 94158, United States*

David M. Wilson − *Department of Radiology and Biomedical Imaging and Helen Diller Family Comprehensive Cancer Center, University of California, San Francisco, San Francisco, California 94158, United States;* orcid.org/0000-0002-1095-046X

Javier E. Villanueva-Meyer − *Department of Radiology and Biomedical Imaging and Helen Diller Family Comprehensive Cancer Center, University of California, San Francisco, San Francisco, California 94158, United States*

https://dx.doi.org/10.1021/acschembio.9b01043
ACS Chem. Biol. 2020, 15, 1381−1391

Jason E. Gestwicki − *Helen Diller Family Comprehensive Cancer Center and Department of Pharmaceutical Chemistry, University of California, San Francisco, San Francisco, California 94158, United States;* orcid.org/0000-0002-6125-3154

Complete contact information is available at: https://pubs.acs.org/10.1021/acschembio.9b01043

Author Contributions

Synthesis of YJH08: Y.H., N.Z., Y.W. *In vitro* affinity assays: Y.H., Y.W., C.T. Radiosynthesis of YJH08: Y.H., N.Z., J.B., H.V.B., D.W. Execution of PET and biodistributions studies: Y.H., N.Z., Y.W., J.W., Y.S. Image reconstruction and analysis: Y.H., Y.S., R.A., S.B., J.V.M. Autoradiography: Y.H., Y.W., J.V.M. Construction of the adipose specific GR KO mouse: M.S., B.F. Synthesis, *in vitro*, and animal studies with JG231: Y.H., H.S., J.G. Supervised the study: M.E.

Notes

The authors declare the following competing financial interest(s): M.J.E. declares an equity stake in ORIC Pharmaceuticals, Inc.

■ ACKNOWLEDGMENTS

We gratefully acknowledge M. James and A. Chaney of Stanford University for assistance with digital autoradiography and T. Huynh for technical assistance with small animal PET/CT studies. M. J. Evans acknowledges funding from the National Institute of Mental Health (R01MH115043) and the Prostate Cancer Research Program of the Congressionally Directed Medical Research Programs (W81XWH-15-1-0552).

■ REFERENCES

(1) Kadmiel, M., and Cidlowski, J. A. (2013) Glucocorticoid receptor signaling in health and disease. *Trends Pharmacol. Sci. 34* (9), 518−30.

(2) Pujols, L., Mullol, J., Roca-Ferrer, J., Torrego, A., Xaubet, A., Cidlowski, J. A., and Picado, C. (2002) Expression of glucocorticoid receptor alpha- and beta-isoforms in human cells and tissues. *Am. J. Physiol: Cell physiol. 283* (4), C1324−31.

(3) Kach, J., Conzen, S. D., and Szmulewitz, R. Z. (2015) Targeting the glucocorticoid receptor in breast and prostate cancers. *Sci. Transl. Med. 7* (305), 305ps19.

(4) Pandey, G. N., Rizavi, H. S., Ren, X., Dwivedi, Y., and Palkovits, M. (2013) Region-specific alterations in glucocorticoid receptor expression in the postmortem brain of teenage suicide victims. *Psychoneuroendocrinology 38* (11), 2628−39.

(5) Webster, M. J., Knable, M. B., O'Grady, J., Orthmann, J., and Weickert, C. S. (2002) Regional specificity of brain glucocorticoid receptor mRNA alterations in subjects with schizophrenia and mood disorders. *Mol. Psychiatry 7* (9), 985−94.

(6) Beattie, B. J., Smith-Jones, P. M., Jhanwar, Y. S., Schoder, H., Schmidtlein, C. R., Morris, M. J., Zanzonico, P., Squire, O., Meirelles, G. S., Finn, R., Namavari, M., Cai, S., Scher, H. I., Larson, S. M., and Humm, J. L. (2010) Pharmacokinetic assessment of the uptake of 16beta-18F-fluoro-5alpha-dihydrotestosterone (FDHT) in prostate tumors as measured by PET. *J. Nucl. Med. 51* (2), 183−92.

(7) Linden, H. M., Stekhova, S. A., Link, J. M., Gralow, J. R., Livingston, R. B., Ellis, G. K., Petra, P. H., Peterson, L. M., Schubert, E. K., Dunnwald, L. K., Krohn, K. A., and Mankoff, D. A. (2006) Quantitative fluoroestradiol positron emission tomography imaging predicts response to endocrine treatment in breast cancer. *J. Clin. Oncol. 24* (18), 2793−9.

(8) Steiniger, B., Kniess, T., Bergmann, R., Pietzsch, J., and Wuest, F. R. (2008) Radiolabeled glucocorticoids as molecular probes for imaging brain glucocorticoid receptors by means of positron emission tomography (PET). *Mini-Rev. Med. Chem. 8* (7), 728−39.

(9) Truillet, C., Parker, M. F. L., Huynh, L. T., Wei, J., Jami, K. M., Wang, Y. H., Shen, Y. S., Sriram, R., Wilson, D. M., Kurhanewicz, J., and Evans, M. J. (2018) Measuring glucocorticoid receptor expression in vivo with PET. *Oncotarget 9* (29), 20399−20408.

(10) Lin, C. W., Nakane, M., Stashko, M., Falls, D., Kuk, J., Miller, L., Huang, R., Tyree, C., Miner, J. N., Rosen, J., Kym, P. R., Coghlan, M. J., Carter, G., and Lane, B. C. (2002) trans-Activation and repression properties of the novel nonsteroid glucocorticoid receptor ligand 2,5-dihydro-9-hydroxy-10-methoxy-2,2,4-trimethyl-5-(1-methylcyclohex-en-3-y1)-1H-[1]benzopyrano[3,4-f]quinoline (A276575) and its four stereoisomers. *Mol. Pharmacol. 62* (2), 297−303.

(11) Coghlan, M. J., Jacobson, P. B., Lane, B., Nakane, M., Lin, C. W., Elmore, S. W., Kym, P. R., Luly, J. R., Carter, G. W., Turner, R., Tyree, C. M., Hu, J., Elgort, M., Rosen, J., and Miner, J. N. (2003) A novel antiinflammatory maintains glucocorticoid efficacy with reduced side effects. *Mol. Endocrinol. 17* (5), 860−9.

(12) Elmore, S. W., Coghlan, M. J., Anderson, D. D., Pratt, J. K., Green, B. E., Wang, A. X., Stashko, M. A., Lin, C. W., Tyree, C. M., Miner, J. N., Jacobson, P. B., Wilcox, D. M., and Lane, B. C. (2001) Nonsteroidal selective glucocorticoid modulators: the effect of C-5 alkyl substitution on the transcriptional activation/repression profile of 2,5-dihydro-10-methoxy-2,2,4-trimethyl-1H-[1]benzopyrano[3,4-f]-quinolines. *J. Med. Chem. 44* (25), 4481−91.

(13) Kym, P. R., Kort, M. E., Coghlan, M. J., Moore, J. L., Tang, R., Ratajczyk, J. D., Larson, D. P., Elmore, S. W., Pratt, J. K., Stashko, M. A., Falls, H. D., Lin, C. W., Nakane, M., Miller, L., Tyree, C. M., Miner, J. N., Jacobson, P. B., Wilcox, D. M., Nguyen, P., and Lane, B. C. (2003) Nonsteroidal selective glucocorticoid modulators: the effect of C-10 substitution on receptor selectivity and functional potency of 5-allyl-2,5-dihydro-2,2,4-trimethyl-1H-[1]benzopyrano[3,4-f]quinolines. *J. Med. Chem. 46* (6), 1016−30.

(14) Zlatopolskiy, B. D., Zischler, J., Krapf, P., Zarrad, F., Urusova, E. A., Kordys, E., Endepols, H., and Neumaier, B. (2015) Copper-mediated aromatic radiofluorination revisited: efficient production of PET tracers on a preparative scale. *Chem. - Eur. J. 21* (15), 5972−9.

(15) Makaravage, K. J., Brooks, A. F., Mossine, A. V., Sanford, M. S., and Scott, P. J. H. (2016) Copper-Mediated Radiofluorination of Arylstannanes with [(18)F]KF. *Org. Lett. 18* (20), 5440−5443.

(16) Coghlan, M. J., Kym, P. R., Elmore, S. W., Wang, A. X., Luly, J. R., Wilcox, D., Stashko, M., Lin, C. W., Miner, J., Tyree, C., Nakane, M., Jacobson, P., and Lane, B. C. (2001) Synthesis and characterization of non-steroidal ligands for the glucocorticoid receptor: selective quinoline derivatives with prednisolone-equivalent functional activity. *J. Med. Chem. 44* (18), 2879−85.

(17) Tredwell, M., Preshlock, S. M., Taylor, N. J., Gruber, S., Huiban, M., Passchier, J., Mercier, J., Genicot, C., and Gouverneur, V. (2014) A general copper-mediated nucleophilic 18F fluorination of arenes. *Angew. Chem., Int. Ed. 53* (30), 7751−5.

(18) Mossine, A. V., Brooks, A. F., Makaravage, K. J., Miller, J. M., Ichiishi, N., Sanford, M. S., and Scott, P. J. (2015) Synthesis of [18F]Arenes via the Copper-Mediated [18F]Fluorination of Boronic Acids. *Org. Lett. 17* (23), 5780−3.

(19) Anacker, C., Zunszain, P. A., Carvalho, L. A., and Pariante, C. M. (2011) The glucocorticoid receptor: pivot of depression and of antidepressant treatment? *Psychoneuroendocrinology 36* (3), 415−25.

(20) Lee, R. A., Harris, C. A., and Wang, J. C. (2018) Glucocorticoid Receptor and Adipocyte Biology. *Nucl. Recept. Res. 5*, DOI: 10.32527/2018/101373.

(21) Sundahl, N., Bridelance, J., Libert, C., De Bosscher, K., and Beck, I. M. (2015) Selective glucocorticoid receptor modulation: New directions with non-steroidal scaffolds. *Pharmacol. Ther. 152*, 28−41.

(22) Shao, H., Li, X., Moses, M. A., Gilbert, L. A., Kalyanaraman, C., Young, Z. T., Chernova, M., Journey, S. N., Weissman, J. S., Hann, B., Jacobson, M. P., Neckers, L., and Gestwicki, J. E. (2018) Exploration of Benzothiazole Rhodacyanines as Allosteric Inhibitors of Protein-Protein Interactions with Heat Shock Protein 70 (Hsp70). *J. Med. Chem. 61* (14), 6163−6177.

(23) Moses, M. A., Kim, Y. S., Rivera-Marquez, G. M., Oshima, N., Watson, M. J., Beebe, K. E., Wells, C., Lee, S., Zuehlke, A. D., Shao, H.,

Bingman, W. E., 3rd, Kumar, V., Malhotra, S. V., Weigel, N. L., Gestwicki, J. E., Trepel, J. B., and Neckers, L. M. (2018) Targeting the Hsp40/Hsp70 Chaperone Axis as a Novel Strategy to Treat Castration-Resistant Prostate Cancer. *Cancer Res. 78* (14), 4022−4035.
(24) Wuest, F., Kniess, T., Bergmann, R., Henry, B., and Pietzsch, J. (2007) Synthesis and radiopharmacological characterization of [11C]AL-438 as a nonsteroidal ligand for imaging brain glucocorticoid receptors. *Bioorg. Med. Chem. Lett. 17* (14), 4035−9.
(25) Eguchi, J., Wang, X., Yu, S., Kershaw, E. E., Chiu, P. C., Dushay, J., Estall, J. L., Klein, U., Maratos-Flier, E., and Rosen, E. D. (2011) Transcriptional control of adipose lipid handling by IRF4. *Cell Metab. 13* (3), 249−59.
(26) Shen, Y., Roh, H. C., Kumari, M., and Rosen, E. D. (2017) Adipocyte glucocorticoid receptor is important in lipolysis and insulin resistance due to exogenous steroids, but not insulin resistance caused by high fat feeding. *Mol. Metab. 6* (10), 1150−1160.

https://dx.doi.org/10.1021/acschembio.9b01043
ACS Chem. Biol. 2020, 15, 1381−1391